Dependence of polaron migration barriers on the fraction of Fock exchange in hybrid functionals

A systematic study of V_k centers in alkali halides

Tygesen, Alexander S.; Chang, Jin Hyun; García-Lastra, Juan María

Published in:
Physical Review B

Link to article, DOI:
10.1103/PhysRevB.108.045120

Publication date:
2023

Document Version
Publisher's PDF, also known as Version of record

Dependence of polaron migration barriers on the fraction of Fock exchange in hybrid functionals: A systematic study of V_k centers in alkali halides

Alexander S. Tygesen, Jin Hyun Chang, and Juan María García-Lastra*
Department of Energy Conversion and Storage, Technical University of Denmark, 2800 Kgs. Lyngby, Denmark

(Received 18 April 2023; revised 22 June 2023; accepted 23 June 2023; published 13 July 2023)

We conduct an exhaustive investigation on the dependence of polaron migrations barriers on the fraction of Fock exchange, α, in hybrid functionals. We analyze different the dependence of different physical quantities on α, such as the band gap of the host material, the fundamental frequency of the polarons, and the polaron localization at the ground and transitions states. We demonstrate that for those systems in which polarons are more (less) localized at their ground state than at their transition state, the migration barriers increase (decrease) on increasing (decreasing) α. By choosing the V_k centers in alkali halides, a paradigmatic example of hole polarons, we show that the α values that reproduce the experimental band gap of the host materials give rise to migration barriers reasonably close to the experimental ones. Surprisingly, we observe that V_k centers' localization behaves differently depending on halide ions. For alkali fluorides, polarons are more localized at the transition state, while for larger halides (Cl, Br, and I) the localization is larger at the ground state.

DOI: 10.1103/PhysRevB.108.045120

I. INTRODUCTION

The mobility of small polarons has been widely studied in the past decades as it plays a crucial role in explaining the electronic transport properties of insulating materials used in various technological applications. Examples of small polarons can be found in materials employed as multiferroics [1], organic light-emitting diodes [2], solid oxide fuel cells [3], and battery cathodes [4–7]. In the case of battery cathode materials, *ab initio* calculations based on density functional theory (DFT) have been carried out to determine small polaron diffusivities, which can serve to estimate the critical thickness of materials for effectively transporting electrons [4,6,8].

Very recently Giustino *et al.* have developed an elegant first-principles method resembling the Bethe-Salpeter equation formalism employed to study excitons in solids [9–11]. Along the same lines, Bernardi *et al.* developed a framework based on canonical transformations for a fast evaluation of polaron formation energies [12]. The beauty of these approaches lies in their ability to describe polaron localization without using supercells. However, these formalisms cannot yet be utilized to study the mobility of polarons. The conventional technique to study polarons through DFT involves using a supercell in which one electron is removed (added) and introducing a compensating homogeneous negative (positive) background charge. The main challenge of this DFT approach is obtaining a solution in which the polaron stays localized in a small region in the supercell rather than completely delocalizing over the entire supercell. The latter tends to occur when DFT exchange-correlation (xc) functionals with a significant self-interaction error (SIE) are employed, such as local-density approximation (LDA) or generalized gradient approximation (GGA). The localized polaron can be described in DFT only if the SIE is sufficiently canceled. Perdew-Zunger self-interaction correction (PZ-SIC) [13], Hubbard correction (i.e., DTU+U) [14], and hybrid functionals [15] can be used for this purpose. The PZ-SIC functional in solids is not widely available across various DFT software packages. For that reason, most of the small polaron calculations in the literature use either the DFT + U approach or hybrid functionals.

Although the Hubbard on-site correction can be obtained through linear response theory [16] and constrained random phase approximation [17], the DFT + U approach is usually considered as semiempirical since many studies set the U correction to match some experimentally observable quantities (e.g., band gap, formation energy, magnetic moments, or lattice parameters) [18]. The main drawback of the DFT + U technique when applied to model polaron mobility is that it may lead to an overestimation of the transition barrier for the polaron hopping [4,19,20]. The overestimation may happen because the U correction stabilizes the energy only by one-half at the transition state compared to the initial (or final) state. This leads to a linear increase of the energy barrier on the U correction [4,20].

In principle, hybrid functionals should not penalize the transition state energy as the DFT + U approach does. Thus, using hybrid functionals has become a standard approach for studying polaron diffusion despite its high computational cost [6,8,19,21–23]. In the hybrid scheme, a fraction of the exchange energy is from the exact-exchange energy from Hartree-Fock (HF) theory, while the remainder comes from the exchange energy from a DFT functional (typically GGA, e.g., PBE [24] for PBE0 [25] and HSE06 [26] or PBEsol [27] for HSEsol [28]). In other words, the hybrid exchange energy, E_x^{hyb}, is expressed as $E_x^{\mathrm{hyb}} = \alpha E_x^{\mathrm{HF}} + (1-\alpha)E_x^{\mathrm{DFT}}$, where E_x^{HF} and E_x^{DFT}, respectively, correspond to the exact-exchange energy from the HF theory and exchange

*jmgla@dtu.dk

energy from a DFT functional. An additional sophistication of hybrid functionals consists of using different α values at short and long ranges. The range separation is set using the μ parameter, which has inverse distance units. The value of μ is set as $0.207\,\text{Å}^{-1}$ for HSE06 and HSEsol, while μ is set as $0.0\,\text{Å}^{-1}$ for PBE0 as it is not a range-separated functional. A default value used for a fraction of the exact exchange, α, is 0.25 in standard PBE0, HSE06, and HSEsol functionals. This default value of $\alpha = 0.25$ was originally chosen based on atomization energies of molecules. [25] However, it has been shown that other α values can provide a better description of atomization energies for solids [29]. In any case the choice of α based on atomization energies is questionable for the study of polarons [30,31].

It has been proven essential to first describe the band gap of material correctly to reproduce the localization of holes [32]. The sensitivity of the appearance of polarons in a material to its band gap is well known, and it has also been proven experimentally. For example, AgCl and AgBr are both rock salt materials with very similar elastic properties, i.e., bulk moduli of AgCl and AgBr are 53.6 GPa and 50.6 GPa, respectively. [33] These two materials have different band gap values, 3.25 eV for AgCl [34] and 2.68 eV for AgBr [34]. Small hole polarons have been observed in AgCl, [35], while the polarons have not been detected in AgBr even when it is cooled down to 1.7 K. [36]

The band gap values increase with a α value in hybrid calculations [31,37]. It has been shown that the optimal α value to match the band gap of a material grows linearly with the inverse of its static dielectric constant, ϵ [37]. Thus, α values around 0.5 generate band gaps close to the experimentally observed values for alkali halides, which have low ϵ values. On the other hand, α values around 0.25 are more appropriate for semiconductors with higher ϵ values [37]. Shimazaki and Asai [38], Marques *et al.* [39], Eisenberg and Baer [40], and Koller *et al.* [37] have proposed approaches in which α is determined based on ϵ. A more practical approach used for studying polarons consists of setting the α value that matches the known band gap values, obtained either from experiments or calculated with the GW method if there are no experimental data [8,21,41].

So far we have outlined how the choice of the U correction in the Hubbard-corrected functionals, and the α parameter in the hybrid functionals affect the localization of polarons. We also mentioned that the magnitude of the U correction in DFT+U also has an impact on the calculated migration barriers of polarons. There is still an open question that we aim to answer in this work: Does α in hybrid functionals influence not only the description of the polaron localization but also its migration barriers? There are clear indications pointing in this direction. One example is the hole polaron in Li_2O_2, where the lowest diffusion barrier calculated with HSE functional with $\alpha = 0.25$ is between 0.038 [21] and 0.068 eV [42], while it is 0.42 eV when $\alpha = 0.48$ [21]. Determining the strong dependence of the migration barrier on α is the first objective of this work. A second question arises on the confirmation of the strong correlation dependence of the migration barrier on α: Does the same α value that yields the best match with the experimental band gap also best estimate the experimentally observed migration barrier? We need to compare our computed polaron migration barriers with the experimental data, which are, unfortunately, scarce.

One of the few examples where systematic studies of polaron migration barriers have been carried out is V_k centers in alkali halides. [43] A V_k center consists of a hole polaron in a X^{2-} dimer formed by two nearest-neighbor halide atoms in a rock salt structure [see Fig. 1(a)]. Castner and Känzig were the first to detect the existence of V_k centers [44]. Since then numerous studies have looked at their mobility [43,45–50]. The diffusion of the V_k centers can occur in 60°, 90°, 120°, and 180° jumps, which correspond to the first, second, third, and fourth nearest neighbors, respectively [46,47,50]. These pathways are depicted in Fig. 1(b). Indeed, Sadigh *et al.* [30] have calculated the diffusion barrier of the V_k center in NaI using the nonscreened PBE0 hybrid functional [25] with the α value that matches the GW calculated band gap, obtaining a barrier in very good agreement with the experimental one.

In the present work, we perform a systematic study of the mobility of V_k centers in 12 alkali halides (alkali: Li, Na, and K; halide: F, Cl, Br, and I) using the PBE0 and HSEsol *xc* functionals, varying the α mixing parameter. This strategy allows us to disentangle the influence of both α and μ parameters on the polaron diffusion barrier. Experimentally, the barriers can be estimated through different techniques, such as nonisothermal electron paramagnetic resonance (EPR) relaxation [51,52] or thermal annealing of optical absorption [53], which can yield slightly different results. We compare our computational results against the experimental values reported by Pung [54], which are obtained using the EPR measurements. To the best of our knowledge, the data by Pung provide the largest set of materials for which the polaron diffusion barriers are measured under the same experimental conditions. Therefore, we opted to compare our results against Pung's data set since using a single experimental source allows for an easier assessment of any eventual systematic deviation between our theoretical results and the experiments.

II. COMPUTATIONAL METHODS

The first step in this work was to determine the α values that match the experimental band gap for both PBE0 and HSEsol *xc* functionals. In the case of the PBE0 functional, Miceli *et al.* [31] reported the band gap of all the Li and Na halides studied in the present work using at least two different α values for each compound. Thus, a simple linear extrapolation based on their data allowed us to determine the α value matching the experimental band gap. Regarding the HSEsol functional and the potassium halides using the PBE0 functional, we could not find sufficient data in the literature to perform such an extrapolation. Therefore, we performed calculations using $\alpha = 0, 0.25, 0.48, 0.75$ and interpolated the α values that match the experimental band gap.

The diffusion of the V_k center was simulated in a $4 \times 4 \times 3$ supercell of the primitive cell. This allowed a convenient representation of the 60°, 120°, and 180° diffusions as these paths are all contained within the *xy* plane of the cell. The mirror symmetry of the pathway can be utilized to apply the reflective nudged elastic band (R-NEB) method [55]. In

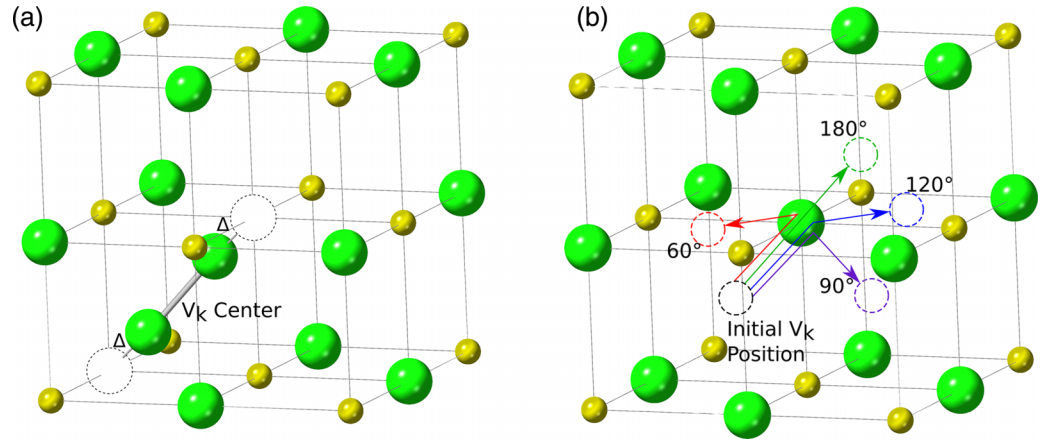

FIG. 1. Illustration of the V_k center and possible diffusion pathways in a cubic rock salt lattice. Alkali ions are illustrated in yellow, and halide ions in green. (a) Two halide ions are compressed by Δ due to a localized hole. (b) Considered diffusion pathways of the V_k center.

the R-NEB, only the first half of the pathway is calculated, while the second half is generated based on symmetry. In this work we applied the reflective middle image NEB (RMI-NEB), an accelerated version of the R-NEB method; it uses a single middle image, which is placed exactly in the mirror plane of the path using linear interpolation. For the 90° jump, it is not possible to construct a symmetrically equivalent initial and final state due to the nonuniform shape of the supercell. Therefore, the 90° pathway was sampled using a regular NEB with three intermediate images.

DFT calculations in this work were performed in the Vienna Ab initio Simulation Package (VASP) [56,57]. The structures were generated using the Atomic Simulation Environment (ASE) [58] software package, which has also been used to perform all RMI-NEB and NEB calculations. Structure relaxations and band gaps were calculated using a k-point density of 3.5 per $Å^{-1}$ in a Γ-centered Monkhorst-Pack grid [59] in the primitive unit cell. RMI-NEB and NEB calculations were carried out on the Γ point to limit the computational costs. Plane-wave cutoffs were selected based on the recommended VASP pseudopotential plane-wave cutoff energies. The cutoff values are dependent on the elements in the structure, and the values used in this study are listed in Table I. A smearing of 0.01 eV was applied for the occupation of the electronic states, and all calculations were performed as spin-polarized. The total energies were converged to 10^{-5} eV or less in the self-consistent field (SCF) cycle. The NEB calculations were run until the projected forces were less than 0.05 eV $Å^{-1}$. Introducing a V_k center accompanies the removal of an electron, which causes the cell to have a net charge. The hole is compensated by a homogeneous background charge in order to avoid infinite charge due to the periodic boundary conditions [60]. In addition, we also studied the X_2^- molecules *in vacuo* using a 6 Å × 6 Å × 20 Å unit cell in which the molecules were oriented in the z direction.

As a validation test of the RMI-NEB method and the size of the 4 × 4 × 3 primitive cell (96 atoms in the supercell) used in the present work, we compared our results with those computed by Sadigh *et al.* [30] for the 60°, 120°, and 180° polaron migration barriers in NaI. In order to obtain migration barriers, Sadigh *et al.* applied the climbing image nudged elastic band method [61] in a 3 × 3 × 3 conventional cell size (216 atoms in the supercell), taking $a = 6.407$ Å as lattice parameter and a modified PBE0 functional with $\alpha = 0.31$. Using the same lattice parameter and α value, our approach yielded energy barriers slightly larger (by 0.005 eV to 0.02 eV) than those reported by Sadigh *et al.* (see Table II). Given the small differences, we considered our approach validated.

In order to get a deeper insight into the nature of the V_k centers and their configuration at the transition state, we carried out a set of molecular calculations of X_2^- and X_3^{2-} molecules, which represent the V_k center at the initial state and at the transition state, respectively. These molecular calculations were carried out using the 2020 version of Amsterdam Density Functional (ADF) software [62] using an all-electron quadruple-ζ four-polarized (QZ4P) basis set and a COnductor-like Screening MOdel (COSMO) [63].

TABLE I. Plane-wave cutoff energies (in eV) for the considered systems.

	Li	Na	K
F	600	550	550
Cl	650	350	350
Br	650	350	350
I	650	350	350

TABLE II. Energy barriers calculated in this work for the polaron diffusion along 60°, 120°, and 180° angles in NaI using the PBE0 functional with different α values and lattice parameters. Results obtained by Sadigh *et al.* [30] for the same system are shown in the last column.

	Present work				Sadigh *et al.*
α	0.35	0.31	0.35	0.31	0.31
a (Å)	6.456	6.456	6.407	6.407	6.407
60° barrier (eV)	0.291	0.261	0.266	0.234	0.23
120° barrier (eV)	0.305	0.275	0.284	0.251	0.23
180° barrier (eV)	0.291	0.261	0.266	0.230	0.22

TABLE III. Computed and experimental band gaps in eV. The α values in HSEsol and PBE0 are varied from 0 to 0.75. The last column shows the interpolated α^{opt} values that match the experimental band gaps.

		Band gap (eV)					α^{opt}
		$\alpha = 0$	$\alpha = 0.25$	$\alpha = 0.48$	$\alpha = 0.75$	Exp.	
LiF	HSEsol	9.0	11.8	14.3	17.4	14.5 [65]	0.49
	PBE0	–	–	–	–		0.51[a]
LiCl	HSEsol	6.4	7.9	9.3	11.0	9.4 [66]	0.49
	PBE0	–	–	–	–		0.37[a]
LiBr	HSEsol	5.0	6.3	7.5	9.1	7.6 [66]	0.49
	PBE0	–	–	–	–		0.35[a]
LiI	HSEsol	4.3	5.3	6.2	7.4	6.1 [67]	0.44
	PBE0	–	–	–	–		0.29[a]
NaF	HSEsol	6.2	8.5	10.7	13.5	11.5 [66]	0.55
	PBE0	–	–	–	–		0.47[a]
NaCl	HSEsol	5.0	6.5	7.8	9.5	9.0 [66]	0.67
	PBE0	–	–	–	–		0.49[a]
NaBr	HSEsol	4.1	5.4	6.6	8.0	7.0 [68]	0.56
	PBE0	–	–	–	–		0.37[a]
NaI	HSEsol	3.6	4.6	5.6	6.9	5.9 [66]	0.52
	PBE0	–	–	–	–		0.35[a]
KF	HSEsol	6.1	8.2	10.3	12.8	10.9 [69]	0.54
	PBE0	5.7	8.9	11.6	15.0		0.42
KCl	HSEsol	5.1	6.4	7.7	9.3	8.7 [70]	0.65
	PBE0	5.0	7.2	9.2	11.5		0.425
KBr	HSEsol	4.3	5.5	6.7	8.0	7.3 [68]	0.60
	PBE0	4.3	6.3	8.1	10.3		0.38
KI	HSEsol	3.9	4.9	5.9	7.1	5.9 [71]	0.49
	PBE0	3.8	5.6	7.2	9.2		0.30

[a]Interpolation from PBE0 band gaps in Miceli *et al.* [31].

III. RESULTS AND DISCUSSION

A. Band gaps of the perfect crystals

The dependence of the band gap of the studied alkali halides on the α value for the HSEsol and PBE0 functionals is shown in Table III. In good agreement with previous studies [31,37,64], we observe a linear increase of the band gap with α, which allows a straightforward interpolation to find the optimal α value matching the experimental band gap, α^{opt}. Also in accordance with the report by Miceli *et al.* [31], we observe that the band gaps are larger for PBE0 than for HSEsol for the same α value, as $\mu = 0$ in the former and $\mu = 0.207$ in the latter. This systematic difference in band gaps leads to α^{opt} values considerably smaller for PBE0 than for HSEsol (with the only exception of LiF, where α^{opt} is similar for both functionals).

B. V_k center structure

We now look at structures containing the V_k center obtained by relaxing the positions of all atoms in the cell with an added electronic hole. The bond length of the X_2^- species is shown in Table IV for the corresponding PBE0 and HSEsol α^{opt} values. The bond lengths obtained at α^{opt} with PBE0 are systematically longer than those calculated with HSEsol by 3 to 5 pm, which is related to the fact that α^{opt} is always significantly larger for HSEsol than for PBE0. The only exception for this trend is LiF, where both the bond lengths and the α^{opt} values are practically the same for PBE0 and HSEsol. This dependency of the bond length on α is better illustrated in Fig. 2, where a linear decrease in the X_2^- distance *in vacuo* on increasing α is observed (see also Table IV, where data for HSEsol calculations at $\alpha = 0.48$ and $\alpha = 0.75$ are listed). The inversely proportional relationship between α and X_2^- bond length is expected since the higher α values favor the electron localization, leading to shorter bond lengths.

TABLE IV. Computed bond lengths (in Å) of the X_2^- species as V_k centers in alkali halides using PBE0 and HSEsol functionals at their corresponding α^{opt}. We also provide the HSEsol-calculated bond lengths for $\alpha = 0.48$ and $\alpha = 0.75$ values for X_2^- species both as V_k centers in alkali halides and *in vacuo*. For the calculations in vacuo we also report in parentheses the calculated X_2^- vibrational frequencies (in cm^{-1}).

	PBE0	HSEsol		
	α^{opt}	α^{opt}	$\alpha = 0.48$	$\alpha = 0.75$
F_2^-	–	–	1.920 (433.3)	1.879 (482.2)
LiF	1.929	1.922	1.922	1.885
NaF	1.954	1.918	1.928	1.888
KF	1.951	1.909	1.921	1.885
Cl_2^-	–	–	2.562 (241.0)	2.537 (263.4)
LiCl	2.621	2.571	2.571	2.546
NaCl	2.605	2.568	2.580	2.556
KCl	2.604	2.560	2.576	2.557
Br_2^-	–	–	2.805 (143.9)	2.782 (160.2)
LiBr	2.894	2.854	2.854	2.806
NaBr	2.883	2.843	2.840	2.839
KBr	2.865	2.815	2.824	2.802
I_2^-	–	–	3.153 (103.1)	3.133 (117.0)
LiI	3.280	3.238	3.224	3.171
NaI	3.248	3.213	3.195	3.188
KI	3.252	3.195	3.195	3.166

Unfortunately, experimentally measured bond lengths of V_k centers are scarce, making it difficult to compare our computational results with those from the literature. To the best of our knowledge, the only experimentally measured bond length of the X_2^- species in the gas phase is for I_2^-, which was determined to be 3.205 Å through femtosecond photoelectron spectroscopy experiments [72]. On the other hand, there are more experimentally measured data on the fundamental frequencies of the X_2^- species. We remark that the fundamental frequencies are directly connected with the energy required to stretch the X_2^- bond, and, thus, they are a good starting point for a correct description of the diffusion barriers. The available fundamental frequencies of X_2^- from the literature are consolidated in Table V.

It is well known that a reduction in the bond lengths due to hydrostatic or chemical pressure leads to an increase in its vibrational frequencies [77]. In the case of Cl_2^-, the measured fundamental frequency is the same within the experimental error for NaCl, KCl, and RbCl, indicating that the host lattice has a little influence on the bond length of Cl_2^-. Both PBE0 and HSEsol calculations are able to capture this fact: The variation of the Cl_2^- bond length is less than 1 pm in the

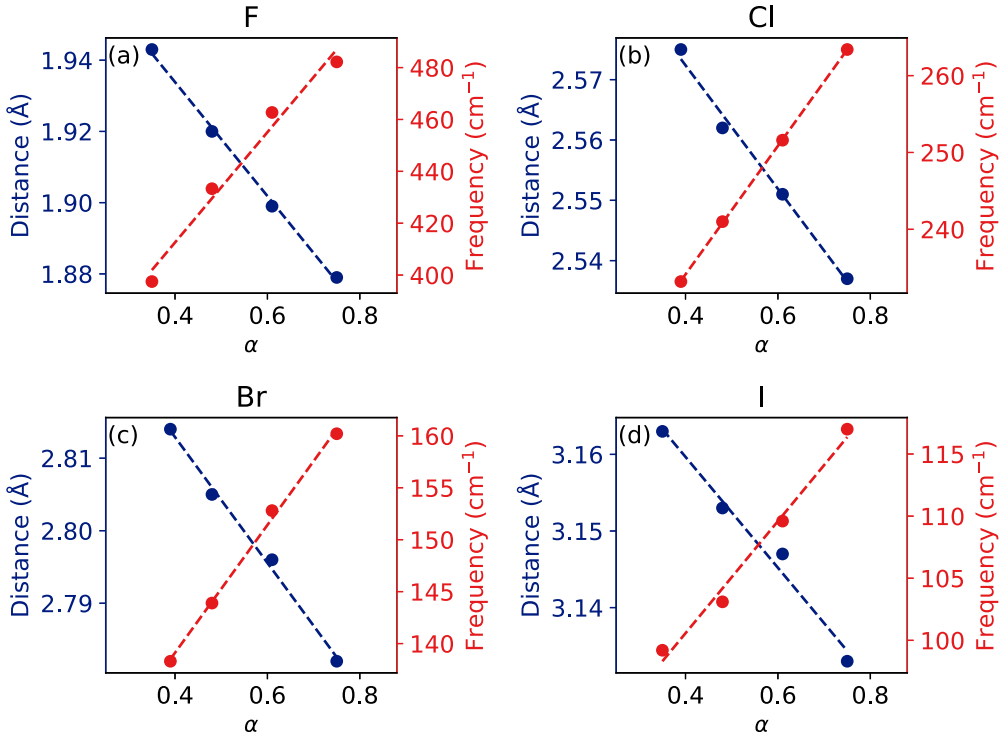

FIG. 2. Dependence of the bond length and the fundamental frequency on α for the X_2^- dimers *in vacuo* calculated with the HSEsol functional.

alkali chloride series. In the case of Br_2^-, the fundamental frequency of KBr is slightly higher (7 cm^{-1}) than that of NaBr, indicating that the bond length of Br_2^- may be a bit longer in NaBr. Our calculations, with both PBE0 and HSEsol functionals, agree with this observation, showing that the Br_2^- bond length is between 1.5 and 3 pm longer in NaBr than in KBr.

The fundamental frequency has a linear dependency on α as shown in Fig. 2, which allows one to find the α value that matches the experimental fundamental frequency and we. We refer to such α value as α^{vib}, and the procedure of determining it using interpolation is the same as finding α^{opt} described in the subsection on band gaps. Table VI shows a comparison between the α^{vib} and α^{opt} for the five alkali halides where experimental fundamental frequencies are available. It can be observed that α^{vib} is nearly independent of the functional choice (i.e., HSEsol or PBE0). However, while α^{vib} and α^{opt} are very close for PBE0 (the mean difference of 0.028), there is a substantial deviation for HSEsol (the mean difference of 0.134). Although we should be cautious since we have experimental data only for five out of the 12 systems studied here, it seems reasonable to state that PBE0 outperforms HSEsol in describing the diffusion barriers in alkali halides based on the similarity between α^{vib} and α^{opt}.

TABLE V. Experimentally measured fundamental frequencies (in cm^{-1}) of the X_2^- species as V_k centers in alkali halides or in gas phase. Although V_k centers in Rb halides are not studied in the present work, we have included experimental data on RbCl for comparison purposes. In NaCl the Raman signal splits in two peaks located at 258 cm^{-1} and 228 cm^{-1} [73], and the average value of the two is 243 cm^{-1}.

	F	Cl	Br	I
Li	437 [74]	–	–	–
Na	–	243 [73]	137 [75]	–
K	–	241 [74]	144 [76]	–
Rb	–	244 [74]	–	–
Gas phase	–	–	–	110 [72]

C. Diffusion barriers

The transition state barriers of the V_k center are calculated using the RMI-NEB and NEB methods for 60°, 90°, 120°, and 180° jumps. The (RMI-)NEB sampling for KCl is illustrated in Fig. 3. It can be seen that the transition barriers of KCl in different directions are equivalent, and the observed trend is in

TABLE VI. Comparison between the α^{vib} and α^{opt} values for five alkali halides where experimental fundamental frequencies are available.

	HSEsol		PBE0	
	α^{vib}	α^{opt}	α^{vib}	α^{opt}
LiF	0.52	0.49	0.53	0.51
NaCl	0.51	0.67	0.48	0.49
KCl	0.48	0.65	0.46	0.425
NaBr	0.37	0.56	0.37	0.37
KBr	0.48	0.60	0.45	0.38

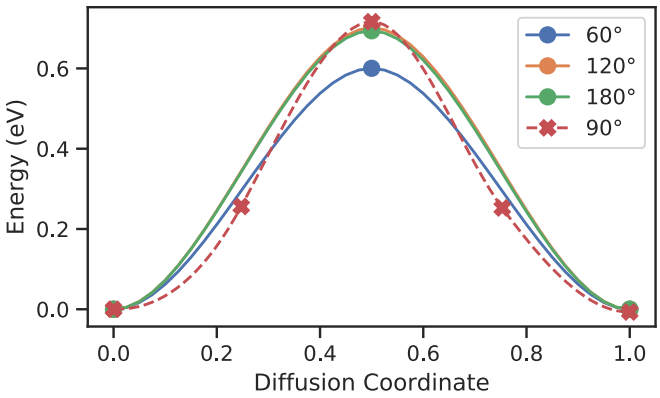

FIG. 3. Diffusion of V_k centers in KCl with $\alpha = 0.48$. The 60°, 120°, and 180° jumps are sampled using a single image with RMI-NEB, and the 90° jump is sampled with a regular NEB with three intermediate images.

good agreement with what was already known from previous experimental and theoretical studies [49,50].

The transition state barriers of the full spectrum of alkali halides are shown in Table VII. We tackle the first question posed in the Introduction about the influence of the α value on the migration barrier. We attempted to compute the migration barriers using HSEsol for $\alpha = 0$, $\alpha = 0.25$, $\alpha = 0.48$, and $\alpha = 0.75$. The results reported in Table VII have transition state barriers only for $\alpha = 0.48$ and $\alpha = 0.75$ due to the computational difficulties for $\alpha = 0$ and $\alpha = 0.25$. The V_k centers do not localize for any of the systems for $\alpha = 0$ (plain PBE). For the $\alpha = 0.25$ case, V_k centers localize for all the alkali halides except for LiBr and LiI, but the hole polaron delocalized at the transition state for a substantial portion of the cases (LiBr, LiI, NaF, NaCl, NaBr, NaI, and KF). In view of these localization problems for low α values, we focused our analysis on the results for $\alpha = 0.48$ and $\alpha = 0.75$.

The dependence of the migration barrier on α varies significantly among the four halides. Fluorides exhibit a drastic reduction of the barrier when α is increased from 0.48 to 0.75 (for the case of NaF, there is even no barrier at $\alpha = 0.75$). The barrier reduction is also found for chlorides but at a much milder level. The barriers are, on average, practically the same for bromides (i.e., a slight reduction of barriers for some, while a slight increase for others). Finally, a small increase in barriers is observed for the iodides. How can we rationalize these trends? Why do the barriers in fluorides have such a peculiar behavior? We remark that our initial hypothesis based on HSE results of hole polarons in Li_2O_2 and DFT + U studies in Li_2O_2 and transition metal phosphates was the opposite, i.e., the migration barrier will increase as α becomes larger.

It is expected that the dependence of the migration barriers on α is related to the relative degree of localization of the unpaired electrons in the V_k center at the initial state vs the transition state. Thus, to answer the questions above, we look at the molecular orbitals of the V_k center and the transition state for the 180° jumps. The ground state of a V_k center, X_2^-, is $^2\Sigma_u^+$ with the $\sigma_2^g\pi_4^u\pi_4^g\sigma_1^u$ occupation, while the transition state of the X_3^{2-} species is $^2\Sigma_u^+$ with the $\sigma_2^u\pi_4^u\sigma_2^g\pi_4^g\pi_4^u\sigma_1^u$ occupation. The pictorial representation of the relevant σ orbitals to understand the dependence of the barrier on α is shown in Fig. 4.

TABLE VII. Computed transition state barriers (in eV) of 60°, 90°, 120°, and 180° jumps for PBE0 and HSEsol α^{opt} and for HSEsol $\alpha \in \{0.48, 0.75\}$ in HSEsol. Experimental barriers are by Pung [54]. No experimental barrier was found for LiI. The boldface denotes the minimum energy jump for each system.

System	Exp.	Angle (°)	PBE0	HSEsol		
			α^{opt}	α^{opt}	$\alpha = 0.48$	$\alpha = 0.75$
LiF	0.28	60	0.27	0.35	0.35	0.16
		120	0.27	0.35	0.35	0.16
		180	**0.26**	**0.34**	0.34	0.16
NaF	0.32	60	0.43	0.39	0.48	0.00
		120	**0.42**	**0.38**	0.47	0.00
		180	0.43	0.38	0.48	0.00
KF	0.34	60	0.59	0.47	0.56	0.06
		90	–	–	0.56	–
		120	**0.58**	**0.47**	0.57	0.07
		180	0.60	0.47	0.56	0.07
LiCl	0.29	60	0.33	0.33	0.33	0.28
		120	0.32	0.30	0.30	0.29
		180	**0.28**	**0.26**	0.26	0.25
NaCl	0.44	60	**0.45**	**0.44**	0.46	0.38
		120	0.49	0.47	0.49	0.39
		180	0.48	0.44	0.49	0.38
KCl	0.54	60	**0.58**	**0.59**	0.60	0.51
		90	–	–	0.72	–
		120	0.67	0.61	0.70	0.52
		180	0.65	0.60	0.69	0.51
LiBr	0.23	60	0.26	0.28	0.28	0.29
		120	0.25	0.25	0.25	0.28
		180	**0.21**	**0.21**	0.21	0.25
NaBr	0.25	60	**0.35**	**0.41**	0.37	0.36
		120	0.38	0.44	0.40	0.37
		180	0.37	0.43	0.39	0.35
KBr	0.43	60	**0.48**	**0.55**	0.49	0.50
		90	–	–	0.60	–
		120	0.56	0.64	0.61	0.54
		180	0.58	0.63	0.63	0.52
LiI	–	60	0.17	0.22	0.24	0.29
		120	0.17	0.21	0.22	0.27
		180	**0.13**	**0.16**	0.16	0.21
NaI	0.18	60	0.29	0.35	0.33	0.37
		120	0.31	0.34	0.33	0.38
		180	**0.29**	**0.34**	0.32	0.36
KI	0.27	60	**0.36**	**0.42**	0.42	0.46
		90	–	0.54	0.54	–
		120	0.42	0.48	0.48	0.53
		180	0.43	0.55	0.55	0.52

For the V_k centers, we find a completely filled bonding σ_g orbital and a partially filled antibonding σ_u^* orbital. The symmetry imposes that $\sigma_g = \frac{1}{\sqrt{2}}(p_z^1 - p_z^2)$ and $\sigma_u^* = \frac{1}{\sqrt{2}}(p_z^1 + p_z^2)$, where i in p_z^i refers to the atom index in the dimer. For the case of the transition state of the X_3^{2-}

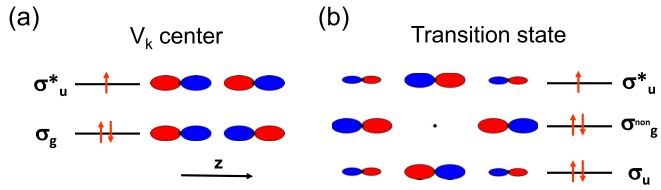

FIG. 4. Orbital occupations of (a) the V_k center X_2^- and (b) the transition state for the 180° jumps (X_3^{2-} species) in their ground state. For simplicity, the π orbitals are omitted, showing only the σ orbitals.

species, the bonding σ_u orbital and the nonbonding σ_g^{non} orbital are fully occupied, and the antibonding σ_u^* orbital is half occupied. In this case the symmetry imposes that $\sigma_u = \frac{\gamma}{\sqrt{2}}(p_z^1 + p_z^3) - \sqrt{1-\gamma^2}p_z^2$, $\sigma_g^{\text{non}} = \frac{1}{\sqrt{2}}(p_z^1 - p_z^3)$, and $\sigma_u^* = \sqrt{\frac{1-\gamma^2}{2}}(p_z^1 + p_z^3) + \gamma p_z^2$, where the $i = 1, 3$ in p_z^i refers to the edge atoms in the trimer and $i = 2$ to the central atom. As it can be seen, the only degree of freedom in these orbital compositions is γ, i.e., the σ_u^* wave-function weight in the central atom of the trimer.

To rationalize the dependence of the migration barrier on α and its relationship with the electron localization (i.e., the γ parameter), we performed a set of calculations for the isolated X_2^- dimers and X_3^{2-} trimers. As stated in the Methods section, we used ADF code to facilitate the analysis of the localization. We first optimized the structure of the dimers and trimers. The $D_{\infty h}$ symmetry is imposed for trimers, i.e., a linear geometry with the middle atom exactly at the center of the trimer as in Fig. 4. These calculations require the use of a solvent model (e.g., COSMO) as the calculations do not converge otherwise. The results of the optimized halide-halide distances using the PBE0 functional in ADF are listed in Table VIII. The results obtained using ADF for the X_2^- dimers are very similar to those presented in Table IV for the isolated dimers calculated with HSEsol in VASP, showing the consistency of the model.

An insightful parameter to obtain from the ADF molecular calculations to obtain the trends in the energy barrier is the dissociation energy, E_d, of a X_3^{2-} trimer into a X_2^- dimer and a X^- anion. With all due caution, the X_3^{2-} trimer resembles the species at the transition state of the V_k center migration, while the X_2^- dimer plus X^- anion resembles the initial (or final)

TABLE VIII. Calculated halide-halide distances, d, of isolated X_2^- dimers and X_3^{2-} trimers (in Å), dissociation energies, E_d, of X_3^{2-} trimers into a X_2^- dimer and an isolated X^- anion, γ^2, and Δ_{SI} $[\sigma_u^{TS} - \sigma_g^{V_K}]$ parameters (see the main text for their definitions).

	α	$d(X_2^-)$	$d(X_3^{2-})$	E_d	γ^2	Δ_{SI} (eV)
F	0.48	1.882	2.201	0.377	0.925	3.180
	0.75	1.837	2.354	0.077	0.972	4.142
Cl	0.48	2.550	2.848	0.266	0.703	−0.516
	0.75	2.512	2.874	0.275	0.778	−0.319
Br	0.48	2.809	3.085	0.181	0.671	−0.558
	0.75	2.772	3.084	0.207	0.720	−0.494
I	0.48	3.179	3.456	0.112	0.620	−0.573
	0.75	3.140	3.443	0.142	0.657	−0.531

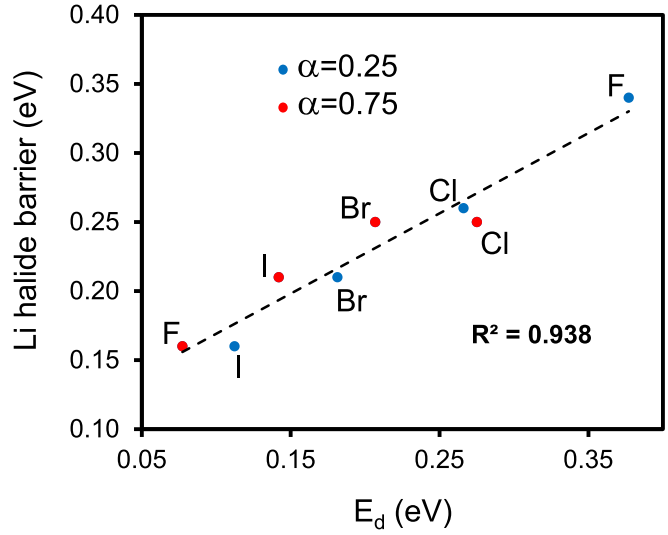

FIG. 5. Comparison of the diffusion barriers for the 180° jumps in the Li halides shown in Table VII vs the dissociation energy of a X_3^{2-} listed in Table VIII.

stage of the migration process. Therefore, E_d could be a good first approximation for the migration energy barriers. Indeed, there is a very good agreement between the calculated energy barriers for the 180° jumps in the Li halides and the E_d (see Fig. 5 for the comparison between the barriers in Table VII and dissociation energies in Table VIII). The agreement is particularly good for Li halides compared to other alkali halides because the COSMO makes a tight solvation of the halide ions, which better resembles the lattices in which the cations are very close to the anions (i.e., the case of the Li halides). The dependence of E_d on α is the same as that of the migration energy barriers: There is a negligible dependence of E_d on α for Cl, Br, and I, while a drastic reduction of E_d is found when α is increased from 0.48 to 0.75 for F. Such a trend is also observed in the halide-halide distances in the X_3^{2-} trimers (see Table VIII): α hardly influences $d(X_3^{2-})$ for Cl, Br, and I while increasing α leads to a significant elongation (>15 pm) of the F-F distance in F_3^{2-}.

Turning back to the electron localization as the ultimate reason to explain the observed trends in the migration barriers, it is instructive to analyze the degree of electron localization in the bonding orbitals of both the V_k center and the transition state (i.e., σ_g and σ_u orbitals for the V_k center and the transition state in Fig. 4, respectively). We choose the self-interaction of the electron in $\sigma_g^{V_k}$ and σ_u^{TS} orbitals as a measure of the electron localization and calculate its dependence on γ (using the Slater-type p orbitals with the exponential decay computed by Roetti and Clementi [78] for each atom type). We then calculated the difference between the self-interaction in the V_k center and the transition state, $\Delta_{SI}[\sigma_u^{TS} - \sigma_g^{V_K}]$, which is plotted in Fig. 6. The electron self-interaction is larger in the transition state than in the V_k center when the γ value is small, i.e., when there is almost no wave function weight in the transition state central ion for its bonding orbital (alternatively, when the induced hole mainly sits in the central ion). When γ increases (beyond 0.2 or 0.3, depending on the specific halide), the situation becomes the opposite, and the

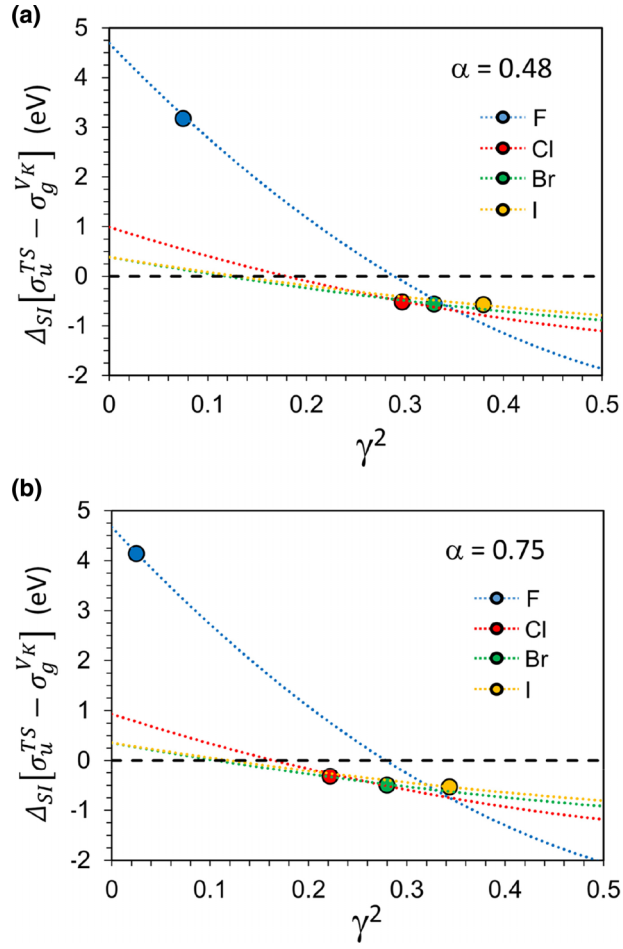

FIG. 6. Dependence of the self-interaction energy difference in the bonding orbitals of X_3^{2-} trimers and X_2^- dimers, $\Delta_{SI}[\sigma_u^{TS} - \sigma_g^{V_K}]$, on γ for the different halides. The filled circles represent the values obtained from the molecular calculations, and the dotted lines are obtained from the analytical calculations.

self-interaction is larger in the V_k center. Since increasing the α in the hybrid functionals reduces the self-interaction error, we can conclude that for small (large) γ values, larger (smaller) α values will reduce (increase) the transition state energies with respect to those of the V_k center.

The actual γ values obtained for the four halides using the molecular calculations, which are shown in Fig. 6 as filled circles for both $\alpha = 0.48$ [Fig. 6(a)] and $\alpha = 0.75$ [Fig. 6(b)]. As expected, there is a small reduction of γ for all the halides when α is increased from 0.48 to 0.75. Since the variations of γ are small, we select the results for $\alpha = 0.75$ [Fig. 6(b)] for further discussion. We observe that γ is very small for F, and thus, $\Delta_{SI}[\sigma_u^{TS} - \sigma_g^{V_K}]$ is large and positive, which explains the drastic reduction in the barriers when α is increased from 0.48 to 0.75. For the other three halides, $\Delta_{SI}[\sigma_u^{TS} - \sigma_g^{V_K}]$ is small and negative, decreasing from Cl to Br and from Br to I. This trend is qualitatively in good agreement with the observed change in barriers when α is increased from 0.48 to 0.75 (i.e., a small decrease, barely any change, and a small increase for Cl, Br, and I, respectively).

The correlation between $\Delta_{SI}[\sigma_u^{TS} - \sigma_g^{V_K}]$ and the average change in the barriers when α is increased from 0.48 to 0.75, $\overline{\Delta B}_{\alpha=0.48\rightarrow0.75}$, is depicted in Fig. 7. Although a good correlation is found, the results shown in Fig. 7 indicate that $\Delta_{SI}[\sigma_u^{TS} - \sigma_g^{V_K}]$ is not the only factor that determines the barrier change; if it was, $\Delta_{SI}[\sigma_u^{TS} - \sigma_g^{V_K}]$ would be slightly positive for Cl, close to zero for Br, and slightly negative for I. Regardless, we have obviated the effect of the V_k center fundamental frequency change when α varies. We have shown that higher α values lead to an increase in the fundamental frequencies, which implies that more energy is required in the first stage of the V_k migration (when the V_k bond starts to stretch) if α increases. From the elastic point of view, larger α values will produce larger barriers. If we combine the "electron localization" and "elastic" effects, simply by slightly shifting the $\Delta_{SI}[\sigma_u^{TS} - \sigma_g^{V_K}]$ in Fig. 7 towards more positive values due to the "elastic effect" (we assume that this elastic influence from α is similar for all the halides), we will be able to rationalize the observed dependence of the barriers on α for all the halide series.

We now look at the suitability of using α^{opt} value for calculating the diffusion barriers by assessing their values against the experimental ones. The computational and experimental barrier data from Table VII are visualized in Fig. 8 for a direct comparison. We observe that the overall experimental trends are well captured by both functionals, although the mean absolute error (MAE) is lower for PBE0 (MAE = 72 meV) than for HSEsol (MAE = 85 meV). The difference becomes more pronounced if we exclude the KF system, the only notorious outlier for PBE0, from the analysis; the MAE reduces to 55 meV for PBE0 and 81 meV for HSEsol. One possible cause for the lower MAE for PBE0 may be the fact that α^{opt} is closer to α^{vib} for PBE0 than for HSEsol. Considering the fact that (1) small variations in the lattice parameter can lead to a significant change in the computed diffusion barrier (e.g., the reduction of 5 pm in the lattice parameter of NaI leads to a reduction of the barriers of 20 meV to 30 meV as shown in Table II) and (2) we used the computed lattice parameters instead of experimental ones, the MAE obtained with the PBE0 is satisfactory. For PBE0, the diffusion barriers calculated using α^{opt} are in very good agreement with experiments for Li halides, while the computed barriers always overestimate their experimental counterparts for Na and K halides.

D. Nature of the transition state

We have addressed the main objective of this work on rationalizing the dependence of the V_k centers' diffusion barriers on α for various alkali halides. With the collected data and obtained insights, we are in a position to address two secondary but relevant questions on the nature of the transition state: (1) Is the transition state metastable? and (2) Is there any preferential angle for the diffusion of the V_k centers?

In their study of V_k centers in KCl, Shluger *et al.* postulated the existence of a so-called "dielectric" one-center polaron, i.e., a metastable state in which the hole is almost completely localized in a single anion [79]. Shluger *et al.* did not find the one-center polaron to be metastable for KCl. In a subsequent study, Prange *et al.* did not find a metastable solution for the diffusion of V_k centers in NaI either [80]. In the previous section, we remarked that the hole is mainly localized at the central anion at the transition state, particularly for fluorine

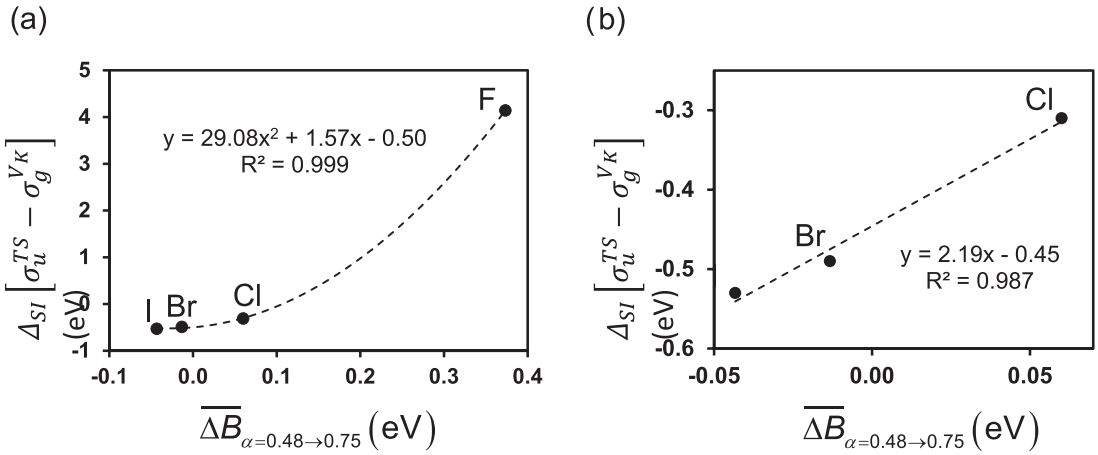

FIG. 7. Correlation between self-interaction energy difference between trimers and dimers and the average change in the barriers when α is increased from 0.48 to 0.75, $\overline{\Delta B}_{\alpha=0.48\to0.75}$, for (a) all four halides and for (b) Cl, Br, and I, where the variation in $\overline{\Delta B}_{\alpha=0.48\to0.75}$ is small.

halides. The localization of the hole primarily in the central anion indicates that the nature of the transition state is indeed the "dielectric" one-center polaron. However, are these one-center polarons metastable? To answer this question, we carried out NEB calculations on the potassium halides with three images between the initial and transition states, i.e., the first half of the path. The sampling of the first half of the diffusion pathways for KF and KCl is shown in Fig. 9. It can be seen that the minimum energy path has a bell shape for KCl, indicating that the transition state is not metastable, which agrees with the results reported by Shluger *et al.* [79]. While they are not shown, the same trend is found for KBr and KI. In contrast, the original transition state of KF, the rightmost point of the diffusion pathway in Fig. 9(b), is a local minimum. The actual transition state is the state between the hole being in a distorted V_k center, indicating that the one-center polaron is indeed metastable in alkali fluorides.

The experimental information on the preferential angle of the V_k center diffusion is scarce. Popp and Murray reported that the most frequent jump in NaI is at 60° [50]. Modeling results by Prange *et al.* using a cluster approach pointed out that the barrier is the same (differences less than 0.01 eV) for the 60° and 180° directions [80]. This result was confirmed by Sadigh *et al.* using periodic supercell calculations [30]. Our results also show that 60° and 180° are the fastest jumps, with practically the same barriers (the difference is less than 0.01 eV). Some experimental data are available for KCl and KI. For KCl, Keller *et al.* reported the probability of a jump in the 60° direction to be around 100 times more likely than in the 90° direction at temperatures in the 150 K to 160 K range [47]. They also concluded that the barrier for the jump along 60° direction is 0.54 eV, which coincides with the barrier determined by Pung [54], which is used as a reference in Table VII. This implies that the barrier for the jumps along the 90° direction in KCl should be around 0.07 eV larger than along the 60° direction. In this work we calculate that difference to be 0.12 eV, which is in good agreement with the experiment, especially when the large experimental uncertainty is taken into account. For KI, Popp and Murray did not report the ratio between the jumps in different directions but noted that the probability of the jumps along the 60° direction is much larger than along 90° direction [50], which again agrees with our results shown in Table VII.

We observe further trends in our calculated barriers on the various jump angles. For the fluorides, the barriers are independent of the jump angle due to the extreme hole localization in the central anion at the transition state. For the rest of the systems, we observe that the preferential jump

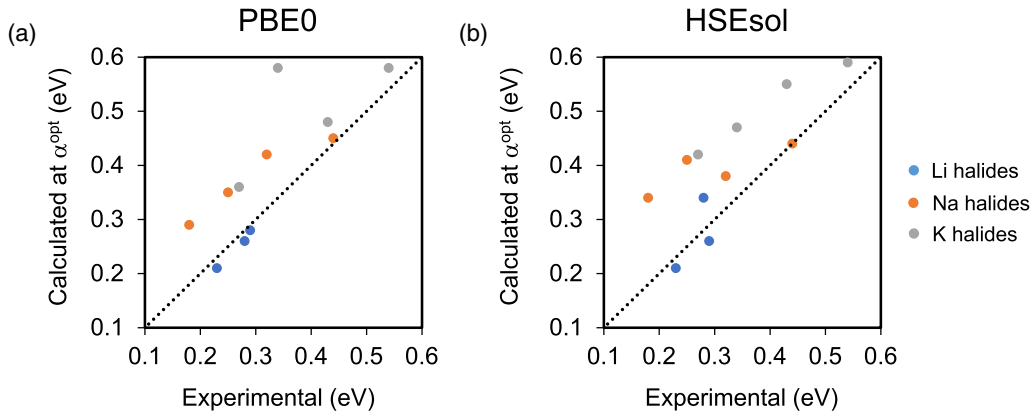

FIG. 8. Comparison between experimental and calculated barriers using α^{opt} for the (a) PBE0 and (b) HSESol functionals.

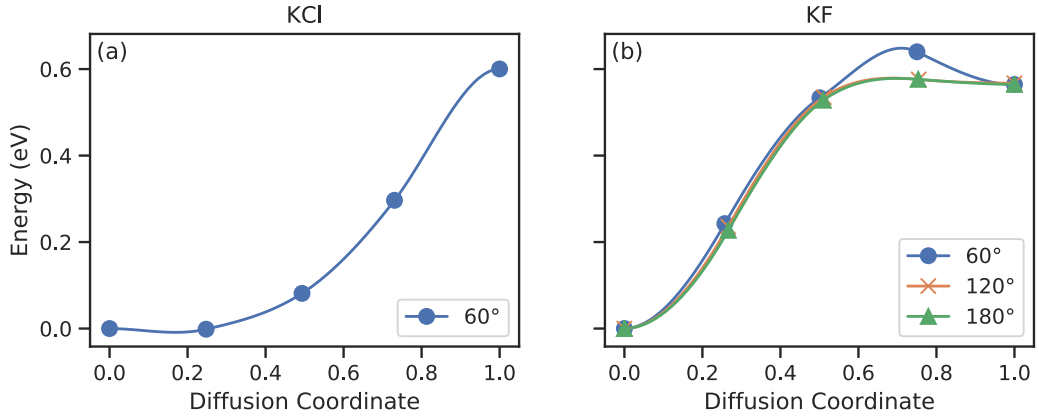

FIG. 9. Increased NEB sampling of the first half of the diffusion pathway of (a) 60° jump for KCl and (b) 60°, 120°, and 180° jumps for KF.

angle barely depends on the halide ions but on the alkali ones, which can be surprising since all the analyzed properties so far have been mostly dependent on the halide ions. For potassium halides, the barriers are always lowest for the 60° jumps. By contrast, the preferred jumps are along the 180° direction for lithium halides. For the sodium halides, the energy differences between the 60° and 180° barriers are very small (0.01 eV) to state anything conclusive. The overall observed trend is that the larger the alkali ion the more preferred the 60° jumps over the 180° jumps. We could not find a straightforward explanation for this observation, and we leave it for future investigations since it is out of the main scope of this work.

IV. CONCLUSIONS

In the Introduction, we posed a question on the dependence of polaron migration barriers on the fraction of Fock exchange, α, in hybrid functionals. We also questioned whether choosing the α value that reproduces the experimental band gap of the host material was also an ideal choice for determining the migration barriers. We decided to use the V_k centers in alkali halides, one of the few cases of polarons for which experimental data on migration barriers had been systematically measured, to help us answer these questions.

Contrary to our expectations, we observed different dependencies of the barriers on α for the various alkali halides. While alkali fluorides suffer a drastic reduction of the barriers on increasing α, the reduction was much weaker for alkali chlorides, and the trend was the opposite for alkali iodides (a slight increase of the barriers on increasing α). Finally, the barriers barely changed for different α values for alkali bromides. We were able to explain this behavior on the basis of the relative hole localization of the ground state vs the transition state, $\Delta_{\mathrm{SI}}[\sigma_u^{TS} - \sigma_g^{V_K}]$, by showing the clear correlation between $\Delta_{\mathrm{SI}}[\sigma_u^{TS} - \sigma_g^{V_K}]$ and the average change in barriers when α is increased from 0.48 to 0.75. A secondary aspect influencing the average change in barriers is the hardening of the fundamental frequencies of the V_k centers on increasing α, a common feature for all the systems studied here. Combining the two effects, i.e., the hole localization and the elastic hardening, we are able to rationalize the barrier variations on changing α.

We show a qualitatively good agreement between the calculated and experimental barriers when using the α that reproduces the band gap of the host material, particularly for the PBE0 functional. Thus, we recommend this procedure, which had already been used in the literature for the study of polaron mobility in Li_2O_2.

To conclude, we were naively expecting that V_k centers would have a similar nature for all the alkali halides before conducting this study. However, we found a much reacher casuistry. The hole is highly localized for fluorides at a single fluorine ion in the transition state. As a salient feature, we found this situation metastable, which had never been reported for V_k centers in alkali halides. For other halides, the localization at the transition state is less pronounced, not being this state metastable.

[1] G. Geneste, C. Paillard, and B. Dkhil, Polarons, vacancies, vacancy associations, and defect states in multiferroic $BiFeO_3$, Phys. Rev. B **99**, 024104 (2019).

[2] V. Coropceanu, J. Cornil, D. A. da Silva Filho, Y. Olivier, R. Silbey, and J. L. Brédas, Charge transport in organic semiconductors, Chem. Rev. **107**, 926 (2007).

[3] J. H. Kim and A. Manthiram, Layered $LnBaCo_2O_{5+\delta}$ perovskite cathodes for solid oxide fuel cells: An overview and perspective, J. Mater. Chem. A **3**, 24195 (2015).

[4] J. M. Garcia-Lastra, J. S. Myrdal, R. Christensen, K. S. Thygesen, and T. Vegge, DFT+U study of polaronic conduction in Li_2O_2 and Li_2CO_3: Implications for Li-Air batteries, J. Phys. Chem. C **117**, 5568 (2013).

[5] M. D. Johannes, K. Hoang, J. L. Allen, and K. Gaskell, Hole polaron formation and migration in olivine phosphate materials, Phys. Rev. B **85**, 115106 (2012).

[6] H. Park, N. Kumar, M. Melander, T. Vegge, J. M. Garcia Lastra, and D. J. Siegel, Adiabatic and nonadiabatic charge transport in Li-S batteries, Chem. Mater. **30**, 915 (2018).

[7] A. Moradabadi and P. Kaghazchi, Effect of Strain on Polaron Hopping and Electronic Conductivity in Bulk $LiCoO_2$, Phys. Rev. Appl. **7**, 064008 (2017).

[8] N. R. Mathiesen, S. Yang, J. M. García-Lastra, T. Vegge, and D. J. Siegel, Charge transport in alkali-metal superoxides: A systematic first-principles study, Chem. Mater. **31**, 9156 (2019).

[9] W. H. Sio, C. Verdi, S. Poncé, and F. Giustino, Polarons from First Principles, without Supercells, Phys. Rev. Lett. **122**, 246403 (2019).

[10] W. H. Sio, C. Verdi, S. Poncé, and F. Giustino, *Ab initio* theory of polarons: Formalism and applications, Phys. Rev. B **99**, 235139 (2019).

[11] J. Lafuente-Bartolome, C. Lian, W. H. Sio, I. G. Gurtubay, A. Eiguren, and F. Giustino, *Ab initio* self-consistent many-body theory of polarons at all couplings, Phys. Rev. B **106**, 075119 (2022).

[12] N.-E. Lee, H.-Y. Chen, J.-J. Zhou, and M. Bernardi, Facile *ab initio* approach for self-localized polarons from canonical transformations, Phys. Rev. Mater. **5**, 063805 (2021).

[13] J. P. Perdew and A. Zunger, Self-interaction correction to density-functional approximations for many-electron systems, Phys. Rev. B **23**, 5048 (1981).

[14] V. I. Anisimov, F. Aryasetiawan, and A. I. Lichtenstein, First-principles calculations of the electronic structure and spectra of strongly correlated systems: The LDA + U method, J. Phys.: Condens. Matter **9**, 767 (1997).

[15] A. D. Becke, A new mixing of Hartree-Fock and local density-functional theories, J. Chem. Phys. **98**, 1372 (1993).

[16] M. Cococcioni and S. de Gironcoli, Linear response approach to the calculation of the effective interaction parameters in the LDA + U method, Phys. Rev. B **71**, 035105 (2005).

[17] F. Aryasetiawan, M. Imada, A. Georges, G. Kotliar, S. Biermann, and A. I. Lichtenstein, Frequency-dependent local interactions and low-energy effective models from electronic structure calculations, Phys. Rev. B **70**, 195104 (2004).

[18] N. J. Mosey and E. A. Carter, *Ab initio* evaluation of coulomb and exchange parameters for DFT + U calculations, Phys. Rev. B **76**, 155123 (2007).

[19] S. P. Ong, V. L. Chevrier, and G. Ceder, Comparison of small polaron migration and phase separation in olivine $LiMnPO_4$ and $LiFePO_4$ using hybrid density functional theory, Phys. Rev. B **83**, 075112 (2011).

[20] T. Maxisch, F. Zhou, and G. Ceder, Ab initio study of the migration of small polarons in olivine Li_xFePO_4 and their association with lithium ions and vacancies, Phys. Rev. B **73**, 104301 (2006).

[21] M. D. Radin and D. J. Siegel, Charge transport in lithium peroxide: Relevance for rechargeable metal-air batteries, Energy Environ. Sci. **6**, 2370 (2013).

[22] H. Shi, R. Jia, and R. I. Eglitis, First-principles calculations of surface *H* centers in BaF_2, Phys. Rev. B **81**, 195101 (2010).

[23] R. Eglitis and A. Popov, Systematic trends in (001) surface *ab initio* calculations of ABO_3 perovskites, J. Saudi Chem. Soc. **22**, 459 (2018).

[24] J. P. Perdew, K. Burke, and M. Ernzerhof, Generalized Gradient Approximation Made Simple, Phys. Rev. Lett. **77**, 3865 (1996).

[25] J. P. Perdew, M. Ernzerhof, and K. Burke, Rationale for mixing exact exchange with density functional approximations, J. Chem. Phys. **105**, 9982 (1996).

[26] A. V. Krukau, O. A. Vydrov, A. F. Izmaylov, and G. E. Scuseria, Influence of the exchange screening parameter on the performance of screened hybrid functionals, J. Chem. Phys. **125**, 224106 (2006).

[27] J. P. Perdew, A. Ruzsinszky, G. I. Csonka, O. A. Vydrov, G. E. Scuseria, L. A. Constantin, X. Zhou, and K. Burke, Restoring the Density-Gradient Expansion for Exchange in Solids and Surfaces, Phys. Rev. Lett. **100**, 136406 (2008).

[28] L. Schimka, J. Harl, and G. Kresse, Improved hybrid functional for solids: The HSEsol functional, J. Chem. Phys. **134**, 024116 (2011).

[29] Y. Meng, X. W. Liu, C. F. Huo, W. P. Guo, D. B. Cao, Q. Peng, A. Dearden, X. Gonze, Y. Yang, J. Wang *et al.*, When density functional approximations meet iron oxides, J. Chem. Theory Comput. **12**, 5132 (2016).

[30] B. Sadigh, P. Erhart, and D. Åberg, Variational polaron self-interaction-corrected total-energy functional for charge excitations in insulators, Phys. Rev. B **92**, 075202 (2015).

[31] G. Miceli, W. Chen, I. Reshetnyak, and A. Pasquarello, Nonempirical hybrid functionals for band gaps and polaronic distortions in solids, Phys. Rev. B **97**, 121112(R) (2018).

[32] S. Loftager, P. Garcia-Fernandez, J. A. Aramburu, M. Moreno, and J. M. Garcia-Lastra, Stability and Polaronic Motion of self-trapped holes in silver halides: Insight through DFT + U calculations, J. Phys. Chem. C **120**, 8509 (2016).

[33] K. F. Loje and D. E. Schuele, The pressure and temperature derivatives of the elastic constants of AgBr and AgCl, J. Phys. Chem. Solids **31**, 2051 (1970).

[34] H. Kanzaki and S. Sakuragi, Optical absorption and luminescence of excitons in silver halides containing isoelectronic impurities. Part II. AgBr:Cl^- and AgBr, J. Phys. Soc. Jpn. **29**, 924 (1970).

[35] E. Laredo, L. G. Rowan, and L. Slifkin, Energy Barrier Against Self-Trapping of the Hole in Silver Chloride, Phys. Rev. Lett. **47**, 384 (1981).

[36] H. Tamura and T. Masumi, Cyclotron resonance of positive holes in AgBr, Solid State Commun. **12**, 1183 (1973).

[37] D. Koller, P. Blaha, and F. Tran, Hybrid functionals for solids with an optimized Hartree-Fock mixing parameter, J. Phys.: Condens. Matter **25**, 435503 (2013).

[38] T. Shimazaki and Y. Asai, Energy band structure calculations based on screened Hartree-Fock exchange method: Si, AlP, AlAs, GaP, and GaAs, J. Chem. Phys. **132**, 224105 (2010).

[39] M. A. L. Marques, J. Vidal, M. J. T. Oliveira, L. Reining, and S. Botti, Density-based mixing parameter for hybrid functionals, Phys. Rev. B **83**, 035119 (2011).

[40] H. R. Eisenberg and R. Baer, A new generalized Kohn–Sham method for fundamental band-gaps in solids, Phys. Chem. Chem. Phys. **11**, 4674 (2009).

[41] H. Park, H. S. Koh, and D. J. Siegel, First-principles study of redox end members in lithium-sulfur batteries, J. Phys. Chem. C **119**, 4675 (2015).

[42] S. P. Ong, Y. Mo, and G. Ceder, Low hole polaron migration barrier in lithium peroxide, Phys. Rev. B **85**, 081105(R) (2012).

[43] P. E. Cade, A. M. Stoneham, and P. W. Tasker, Self-trapped hole (V_k center) in NaCl-type alkali halides. Lattice relaxation and optical properties for MX : X_2^- systems, Phys. Rev. B **30**, 4621 (1984).

[44] T. G. Castner and W. Känzig, The electronic structure of V-centers, J. Phys. Chem. Solids **3**, 178 (1957).

[45] F. J. Keller and R. B. Murray, Preferential Thermal Reorientation of V_k Centers in Potassium Iodide, Phys. Rev. Lett. **15**, 198 (1965).

[46] F. J. Keller and R. B. Murray, Thermal motion of holes in potassium iodide, Phys. Rev. **150**, 670 (1966).
[47] F. J. Keller, R. B. Murray, M. M. Abraham, and R. A. Weeks, Preferential thermal reorientation of V_k centers in potassium chloride, Phys. Rev. **154**, 812 (1967).
[48] K. S. Song, On the migration of V_k-centers in alkali halides, J. Phys. Chem. Solids **31**, 1389 (1970).
[49] K. S. Song, Calculation of activation energy of V_k-centre migration in alkali halides, Solid State Commun. **9**, 1263 (1971).
[50] R. D. Popp and R. B. Murray, Diffusion of the V_k-polaron in alkali halides: Experiments in NaI and RbI, J. Phys. Chem. Solids **33**, 601 (1972).
[51] L. Pung, Non-isothermal epr relaxation and hole recombination luminescence in some ionic crystals, Izv. Akad. Nauk SSSR, Ser. Fiz. **31**, 1968 (1967).
[52] D. Schoemaker, g and hyperfine components of V_K centers, Phys. Rev. B **7**, 786 (1973).
[53] R. B. Murray and F. J. Keller, V_K centers and recombination luminescence in rubidium iodide and sodium iodide, Phys. Rev. **153**, 993 (1967).
[54] L. Pung, The dynamics of nonrelaxed and self-trapped holes in alkali halides, Tr. Inst. Fiz. Akad. Nauk Est. SSR **50**, 7 (1979).
[55] N. R. Mathiesen, H. Jónsson, T. Vegge, and J. M. García-Lastra, R-NEB: Accelerated nudged elastic band calculations by use of reflection symmetry, J. Chem. Theory Comput. **15**, 3215 (2019).
[56] G. Kresse and J. Furthmüller, Efficient iterative schemes for *ab initio* total-energy calculations using a plane-wave basis set, Phys. Rev. B **54**, 11169 (1996).
[57] G. Kresse and D. Joubert, From ultrasoft pseudopotentials to the projector augmented-wave method, Phys. Rev. B **59**, 1758 (1999).
[58] A. H. Larsen, J. J. Mortensen, J. Blomqvist, I. E. Castelli, R. Christensen, M. Dulak, J. Friis, M. N. Groves, B. Hammer, C. Hargus *et al.*, The atomic simulation environment—A Python library for working with atoms, J. Phys.: Condens. Matter **29**, 273002 (2017).
[59] H. J. Monkhorst and J. D. Pack, Special points for Brillonin-zone integrations, Phys. Rev. B **13**, 5188 (1976).
[60] G. Makov and M. C. Payne, Periodic boundary conditions in *ab initio* calculations, Phys. Rev. B **51**, 4014 (1995).
[61] G. Henkelman, B. P. Uberuaga, and H. Jonsson, A climbing image nudged elastic band method for finding saddle points and minimum energy paths, J. Chem. Phys. **113**, 9901 (2000).
[62] G. te Velde, F. M. Bickelhaupt, E. J. Baerends, C. Fonseca Guerra, S. J. A. van Gisbergen, J. G. Snijders, and T. Ziegler, Chemistry with ADF, J. Comput. Chem. **22**, 931 (2001).
[63] C. C. Pye and T. Ziegler, An implementation of the conductor-like screening model of solvation within the Amsterdam density functional package, Theor. Chem. Acc. **101**, 396 (1999).
[64] J. P. Perdew, W. Yang, K. Burke, Z. Yang, E. K. U. Gross, M. Scheffler, G. E. Scuseria, T. M. Henderson, I. Y. Zhang, A. Ruzsinszky *et al.*, Understanding band gaps of solids in generalized Kohn-Sham theory, Proc. Natl. Acad. Sci. USA **114**, 2801 (2017).
[65] M. Piacentini, A new interpretation of the fundamental exciton region in LiF, Solid State Commun. **17**, 697 (1975).
[66] S. T. Pantelides, Electronic excitation energies and the soft-x-ray absorption spectra of alkali halides, Phys. Rev. B **11**, 2391 (1975).
[67] F. C. Brown, C. Gähwiller, H. Fujita, A. B. Kunz, W. Scheifley, and N. Carrera, Extreme-ultraviolet spectra of ionic crystals, Phys. Rev. B **2**, 2126 (1970).
[68] D. Fröhlich and B. Staginnus, New Assignment of the Band Gap in the Alkali Bromides by Two-Photon Spectroscopy, Phys. Rev. Lett. **19**, 496 (1967).
[69] D. M. Roessler and H. J. Lempka, Ultra-violet optical properties of potassium fluoride, Br. J. Appl. Phys. **17**, 1553 (1966).
[70] D. M. Roessler and W. C. Walker, Electronic spectra of crystalline NaCl and KCl, Phys. Rev. **166**, 599 (1968).
[71] W. H. Strehlow and E. L. Cook, Compilation of Energy Band Gaps in Elemental and Binary Compound Semiconductors and Insulators, J. Phys. Chem. Ref. Data **2**, 163 (1973).
[72] M. T. Zanni, T. R. Taylor, B. J. Greenblatt, B. Soep, and D. M. Neumark, Characterization of the I_2^- anion ground state using conventional and femtosecond photoelectron spectroscopy, J. Chem. Phys. **107**, 7613 (1997).
[73] K. Tanimura, T. Suzuki, and N. Itoh, Resonance Raman Scattering of the Self-Trapped Exciton in Alkali Halides, Phys. Rev. Lett. **68**, 635 (1992).
[74] E. Goovaerts and D. Schoemaker, Inelastic light scattering of the V_K centers in the alkali halides, Phys. Status Solidi B **88**, 615 (1978).
[75] T. Suzuki, K. Tanimura, and N. Itoh, Resonance-raman-scattering spectroscopy of the self-trapped excitons in alkali halides, Phys. Rev. B **49**, 7233 (1994).
[76] T. Suzuki, K. Tanimura, and N. Itoh, Resonance-raman-scattering spectroscopy for the halogen-molecular-ion centers in alkali halides, Phys. Rev. B **48**, 9298 (1993).
[77] J. M. García-Lastra, T. Wesolowski, M. T. Barriuso, J. A. Aramburu, and M. Moreno, Optical and vibrational properties of MnF_6^{4-} complexes in cubic fluoroperovskites: Insight through embedding calculations using Kohn–Sham equations with constrained electron density, J. Phys.: Condens. Matter **18**, 1519 (2006).
[78] C. Roetti and E. Clementi, Simple basis sets for molecular wavefunctions containing atoms from $Z = 2$ to $Z = 54$, J. Chem. Phys. **60**, 4725 (1974).
[79] A. L. Shluger, L. N. Kantorovich, E. N. Heifets, E. K. Shidlovskaya, and R. W. Grimes, Theoretical simulation of V_K-centre migration in KCl. I. A quantum-chemical study, J. Phys.: Condens. Matter **4**, 7417 (1992).
[80] M. P. Prange, R. M. Van Ginhoven, N. Govind, and F. Gao, Formation, stability, and mobility of self-trapped excitations in NaI and $NaI_{1-x}Tl_x$ from first principles, Phys. Rev. B **87**, 115101 (2013).